4

# Current Distribution and Stability of a Hybrid Superconducting Conductors Made of LTS/HTS

Yinshun Wang
*Key Laboratory of HV and EMC Beijing, State Key Laboratory for Alternate Electrical Power System with Renewable Energy Sources, North China Electric Power University, Beijing, China*

## 1. Introduction

Although having made great progress in many applications, such as high magnetic field inserts in magnets at helium temperature and electrical engineering application in low magnetic fields at nitrogen temperature, the high temperature superconductor (HTS) is less commercially viable in mid- and large- scale magnets because of its high cost, low engineering critical current density, mechanical brittleness and low n value compared with conventional low temperature superconductors (LTS).

The superconductor with a high n value transfers quicker from superconducting state to the normal conducting state. From the standpoint of application, the transient characteristics strongly affect its stability. With a high current, in the low n value area, flux flow voltage becomes lower than in the high n value area. Generally, it is considered that quenching occurs at a weak point, which is defined as a low $I_c$ and low n value area. However, when such transition is observed, it is predicted that the limit current of quenching will be reached sooner for the high n value than for the lower n value (Torii et al., 2001, Dutoit et al, 1999).

In general, the traditional superconductor has a higher n value than the Bi2223/Ag tape. In order to improve its stability, a LTS is always connected to a conventional conductor with low resistivity and high thermal conductivity, such as copper and aluminum, which then reduces its engineering critical current.

To enhance the performance of conventional composite NbTi superconductors with large current capacity (several tens of kA) utilized in large helical devices (LHD), a new LTS/HTS hybrid in which HTS is used as a part stabilizer in place of low-resistivity metals, was proposed (Wang et al, 2004; Gourab et al, 2006; Nagato et al, 2007). Thus its cryogenic stability against thermal disturbance, steady-state cold-end recovery currents and the minimum propagation currents (MPC) can be greatly improved because the HTS has low resistance and current diffusion which is faster than that in a pure conventional conductor matrix.

$$E = E_c \left( \frac{J}{J_c} \right)^n \tag{1}$$

Based on the power-law model (1) fitted in range of 0.1μV/cm ≤E≤1μV/cm, LTS has a higher n value (≥25) than HTS with a relative lower n value (<18) due to its intrinsic and

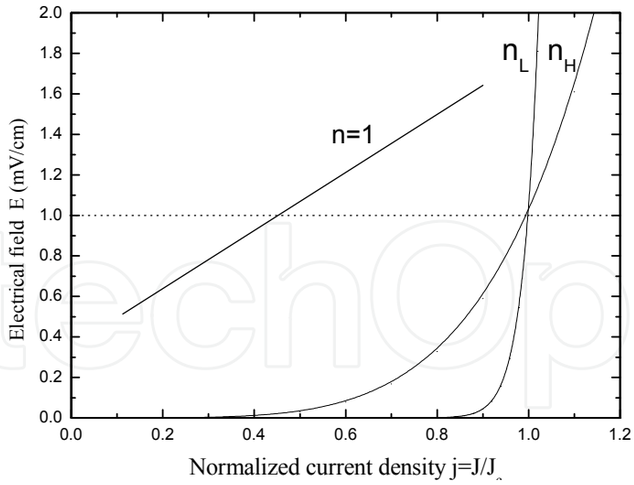


Fig. 1. Schematic E vs J plots of superconductors with $n_H$ and $n_L$($n_L$>$n_H$), normal metal with n=1

granular properties (Yasahiko et al., 1995; Rimikis et al., 2000). According to different n values between LTS and HTS shown as Fig. 1, n=1 refers to the normal conductor according to the Ohm law. We firstly suggested a type of LTS/HTS hybrid composite conductor in 2004 in order to improve the stability of mid- and large scale superconducting magnets, in particular the cryo-cooled conduction superconducting magnet application.

Due to the different n values between LTS and HTS, the transport current flows initially through the LTS in the hybrid conductor. If there is a normal-transition in the LTS with some disturbance, the transport current will immediately transfer to the HTS, then the heat generation can be suppressed and full quench may be avoided. On the other hand, since the thermal capacity of HTS is two orders of magnitude higher than that of LTS, temperature rise can be smaller in the hybrid conductor than in the LTS. Therefore, the hybrid conductor can endure larger disturbances and maintain a higher transport temperature margin. In this chapter, we report on the current distribution and stability of a LTS/HTS hybrid conductor by simulation and experiment near in the range of 4.2K.

## 2. Numerical models of current distribution and stability

### 2.1 Current distribution

This kind of LTS/HTS hybrid conductor consists of soldering LTS wire and HTS tape together or by directly winding several LTS wires and HTS tapes together in parallel mode. The LTS/HTS superconductor is combination of LTS wire and HTS tapes shown in Fig.2.

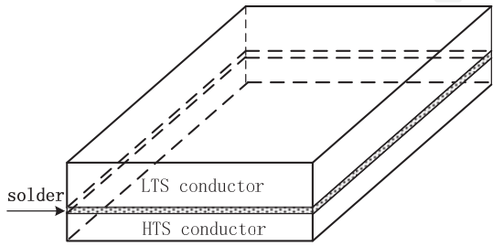


Fig. 2. Schematic view of LTS/HTS hybrid conductor with combination of LTS and HTS conductors

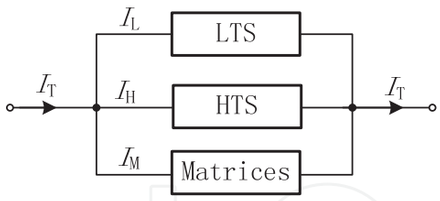


Fig. 3. Equivalent parallel circuit consisting of LTS/HTS hybrid conductor

According to its processing technology, the LTS/HTS hybrid conductor can be approximately considered to be equivalent parallel circuit consisting of LTS, HTS and metal matrix, shown in Fig. 3.

Let $U_H$, $U_L$, $U_M$ be the voltages of the pure HTS, LTS conductors and the normal metal matrix including metal sheath, solder, etc, respectively; and $J_H$, $J_L$, $J_M$ the corresponding branch current densities. Those parameters satisfy the following equations

$$U_H = U_c \left( \frac{J_H}{J_{cH}} \right)^{n_H} \tag{2}$$

$$U_L = U_c \left( \frac{J_L}{J_{cL}} \right)^{n_L} \tag{3}$$

$$U_M = I_M R_M \tag{4}$$

$$U_H = U_L = U_M \tag{5}$$

where $U_c=E_cL_0$, $E_c$ is critical electric field ($E_c$ =E($I_c$)),and is usually equal to 1.0 μV/cm, $L_0$ is the length of the hybrid superconductor, $n_H$ and $n_L$ are the n indices of HTS and LTS, respectively; $J_{cH}$ and $J_{cL}$ are their critical current densities. $R_M$, the resistance of the matrices, is approximately given by

$$R_M = \rho_{avg} \frac{L_0}{S_M} \tag{6}$$

where $\rho_{avg}$ and $S_M$ are the effective resistivity and cross-sections of the matrices, estimation of $\rho_{avg}$ is given , shown as Fig. 5

$$\frac{1}{\rho_{avg}} = \sum_{i=1}^{n} \frac{f_i}{\rho_i} \tag{7}$$

where $f_i$ and $\rho_i$ are volumetric ratio and resistivity of i-th components in matrices except for the LTS and HTS. Since the resistivity of superconductors is more at least one order than the metal conductor, it is reasonable to neglect the resistances of superconductors in this chapter.

Based on Eq. (2) through Eq. (6), following relations are found for unit length of the hybrid conductor

$$\begin{cases} I_T = I_H + I_L + I_M \\ \left(\dfrac{I_H}{I_{cH}}\right)^{n_H} = \left(\dfrac{I_L}{I_{cL}}\right)^{n_L} \\ \left(\dfrac{I_H}{I_{cH}}\right)^{n_H} \times 10^{-4} = R_{avg} I_M \end{cases} \tag{8}$$

where $I_T$ is total transport current of hybrid conductor, and $I_H$, $I_L$ and $I_M$ the transport currents through HTS, LTS and matrices, respectively. The temperature dependence of critical currents of LTS and HTS in the hybrid superconductor can be approximately expressed as polynomial expressions with constant coefficients. Then the current distribution can be simulated according to Eq. (8).

### 2.2 Thermal stability

In order to conveniently analyze the thermal stability of the hybrid superconductor under the adiabatic condition, the heat source, made of heater, is located at the center of conductor with 200 mm length, and the length of heaters along the conductor is 10 mm, as schematically shown in Fig. 4.

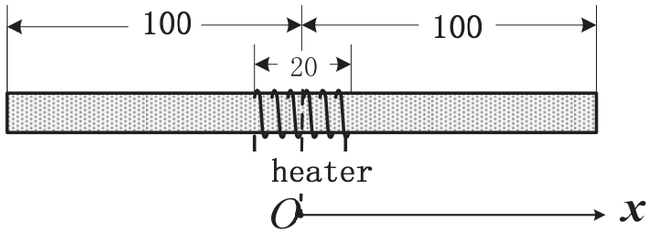


Fig. 4. Schematic view of heating on the hybrid conductor

The length of any segments is much larger than their cross-section and then the physical properties are assumed to be homogeneous over the cross-section. The numerical simulation may be simplified by choosing following one-dimensional, nonlinear, transient, heat balance equation (Wilson, 1983; Iwasa, 1994)

$$(\gamma C)_{avg} \frac{\partial T}{\partial t} = \frac{\partial}{\partial x}\left(k_{avg} \frac{\partial T}{\partial x}\right) + \frac{Q}{V} + \frac{G}{V_0} \tag{9}$$

where $(\gamma C)_{avg}$ is average heat capacity ($J \cdot m^{-3} \cdot K^{-1}$), $k_{avg}$ the average thermal conductivity ($W \cdot m^{-1} \cdot K^{-1}$), Q the joule heat (W) generated in hybrid conductor, G the initial heat disturbance (W) applied by heater, V the total volume of the hybrid conductor and $V_0$ the volume of hybrid conductor surrounded by heater.

Both of average heat capacity and thermal conductivity are estimated according to Fig.5. Assuming that a composite conductor consists of n kinds of material, the heat capacity of each material is $(\gamma_i C_i)$ in which $\gamma_i$ and $C_i$ are mass density and heat specific, respectively, $k_i$ and $\rho_i$ its thermal conductivity and resistivity, the volumetric ratio of each component to

total volume is $f_i$ (i=1,2,⋯n). Fig. 5 is the schematic view of a composite conductor through which the heat Q and current I flow longitudinally. Fig.5 can be equivalent to "serial circuit" models for heat capacity $(\gamma C)_i$ and thermal conductivity $k_i$, but parallel circuit model for resistivity $\rho_i$. Then the maximum averages of heat capacity and thermal conductivity are respectively expressed by

$$(\gamma C)_{avg} = \sum_{i=1}^{n} f_i (\gamma_i C_i) \tag{10}$$

$$k_{avg} = \sum_{i=1}^{n} f_i k_i \tag{11}$$

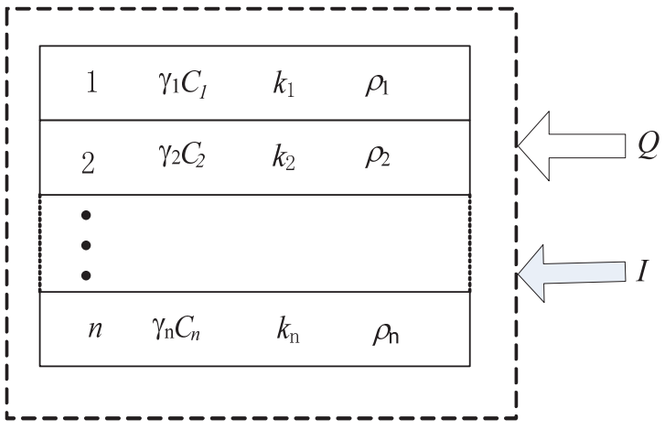


Fig. 5. Overview of a composite conductor with longitudinally flowing heat Q and current I

where $f_i$ is volumetric ratio of each component in hybrid conductors, n the number of components, $\gamma_i$, $C_i$ and $k_i$ are mass density, heat specific and thermal conductivity of i-th components, respectively. In this chapter, 1 refers to copper, 2 represents NbTi, 3 indicates solder, 4 corresponds to YBCO CC for hybrid conductor made of NbTi/Cu conductor and YBCCO CC. On the other hand, 1 refers to copper, 2 represents NbTi, 3 indicates solder, 4, 5, 6 respectively refer to stainless steel, Bi2223 and silver for the one consisted of NbTi/Cu conductor and Bi2223/Ag tape.

In general, if a rectangular pulse disturbance is applied, the heat term G is given by

$$G = \begin{cases} I_g^2 R_g & (0 \le t \le t_g,\ 0 < x \le x_g) \\ 0 & (other\ conditions) \end{cases} \tag{12}$$

where $t_g$ and $x_g$ are the effective time and half length of the heater along the hybrid conductor located its center, here $x_g$=10 mm. $I_g$ and $R_g$ the current going through the heater and its resistance, respectively.

Let $T_{cs}$ be the current sharing temperature, while $T>T_{cs}$, the Joul heat term Q in (W) is generated by

$$Q = I_M^2 R_M \tag{13}$$

When the hybrid conductor operates in superconducting state, $I_M$=0; If $T_{cs}$ <$T_{cL}$, the current distributions are described by

$$I_M = \begin{cases} 0 & (T < T_{cs}) \\ I_T - (I_L + I_H) & (T_{cs} \le T < T_{cL}) \\ I_T - I_H & (T_{cL} \le T < T_{cH}) \\ I_T & (T \ge T_{cH}) \end{cases} \tag{14}$$

Substituting $\frac{\partial T}{\partial t} = \frac{\partial T}{\partial x}\frac{\partial x}{\partial t} = v\frac{\partial T}{\partial x}$ into Eq. (9), we have

$$k_{avg}\frac{\partial^2 T}{\partial x^2} + (\frac{\partial k_{avg}}{\partial x} - v(\gamma C)_{avg})\frac{\partial T}{\partial x} + \frac{Q}{V} + \frac{G}{V_0} = 0 \tag{15}$$

where v is the longitudinal quench propagation velocity (QPV) along the hybrid conductor length.

According to the one-dimensional model shown in Fig. 4, if the environment temperature is in liquid helium, the boundary and initial conditions are given by

$$\begin{cases} \left.\frac{\partial T}{\partial x}\right|_{x=0} = 0 \\ T|_{x=100} = 4.2 \\ T(x)|_{t=0} = 4.2 \end{cases} \tag{16}$$

Based on Eq.(13) through (16), the stability characteristics of the hybrid conductor, such as longitudinal quench propagation velocity (QPV) and minimum quench energy (MQE), can be simulated.

## 3. Simulation and results

In temperature T (<$T_{cL}$), the critical current of this kind of hybrid conductor is defined as

$$I_c(T) = I_{cH}(T) + I_{cL}(T) \tag{17}$$

For the sake of convenience, the normalized transport current $\alpha = I_T/I_c$ is defined and used thereafter. Table 1 lists geometrical and superconducting characteristics of composite NbTi/Cu, Bi2223/Ag by enforced stainless steel, YBCO coated conductor (YBCO CC) and the metal matrices in the hybrid conductor used in the numerical simulation in this paper. The critical currents are given in 4.2 K and magnetic field of 6 T with parallel to their wide surface for reducing their critical currents. In order to make the critical current of HTS comparable with the LTS as soon as possible, two commercial HTS tapes were selected in simulation and experiment (Section 4).

| Material | Description | value |
|---|---|---|
| NbTi/Cu | Width/mm | 4.3/4.5 |
| | Thickness/mm | 0.42/0.58 |
| | Length/mm | 1200 |
| | Cross-section ratio of copper to superconductor | ~1.38 |
| | $I_c$@4.2 K and 6 T | 960A |
| | n value@4.2K and 6 T | 25 |
| YBCO CC laminated on both sides with harden copper | Conductor Width/mm | 4.41 |
| | Conductor Thickness/mm | 0.20 |
| | Length/mm | 1200 |
| | YBCO width/μm | ~1 |
| | Copper stabilizer thickness/mm | ~0.1 |
| | Ic@ 4.2K and 6 T in parallel field (2 tapes) | 2×350A=700A |
| | n value@4.2 K and 6 T | 12 |
| Bi2223/Ag tape enforced by stainless steel | Width/mm | 4.3 |
| | Thickness/mm | 0.29 |
| | Length/mm | 1200 |
| | Stainless-steel thickness/mm | 0.05/each side |
| | Ratio of silver and stainless-steel to superconductor | ~3 |
| | $I_c$@4.2 K and 6 T in parallel field (2 tapes) | 2×293=586A |
| | n value@4.2 K and 6 T | 15 |
| Solder (50Sn and 50Pb) | Width/mm | 4.3 |
| | Thickness/mm | <0.1 |

Table 1. Main parameters of superconductors and solders

### 3.1 Current distribution

#### 3.1.1 Current distribution of hybrid conductor made of NbTi/Cu and YBCO CC

It is assumed that the hybrid conductor be soldered by solder Sn50-Pb50 and so that it is combination of NbTi/Cu with two YBCO CC. Under magnetic field of 6 T, dependence of critical currents of NbTi on temperature can be described by modified Morgan formulae

$$I_c(T) = 960 - 362(T - 4.2) - 17.5(T - 4.2)^2 + 1.85(T - 4.2)^3 \tag{18}$$

In 4.2 K and 6 T, the critical current $I_c$ is 960 A. With parallel magnetic field 6T, the relation of critical current with temperature in two YBCO CC is approximately described by

$$I_c(T) = I_c(0)\left(1 - \frac{T}{T_c}\right)^{1.2} \tag{19}$$

where $I_c(0)$ is critical current with T=0 K and B=6 T, $I_c(0)$=743 A, $T_c$ =93 K is the critical temperature of YBCO CC, $I_c$=700 A is critical currents of two YBCO CC in 4.2 K and 6 T.

Neglecting magnetic field effect, the dependence of resistivity (Ω·m) in Cu and solder (50Sn-50Pb) on temperature are approximately described by

$$\rho_{Cu}(T)=\begin{cases}5.142\times10^{-15}T^3-1.1998\times10^{-14}T^2-1.714\times10^{-14}T+2.208\times10^{-10} & (4K<T\le 60K)\\ 6.856\times10^{-15}T^2+6.6846\times10^{-11}T-2.738\times10^{-9} & (60<T\le 300K)\end{cases} \quad (20)$$

And

$$\rho_{solder}(T)=\begin{cases}-2.15\times10^{-13}T^3+2.0\times10^{-11}T^2-1.2\times10^{-10}T+5.4\times10^{-9} & (4.2K<T\le 45K)\\ 4.85\times10^{-10}T-2.8\times10^{-10} & (45K<T\le 300K)\end{cases} \quad (21)$$

According to Eqs.(2)-(8) and (18)-(21), the current distribution among NbTi, YBCO CC and matrices can be numerically calculated with different transport current I and parallel magnetic field of 6T.

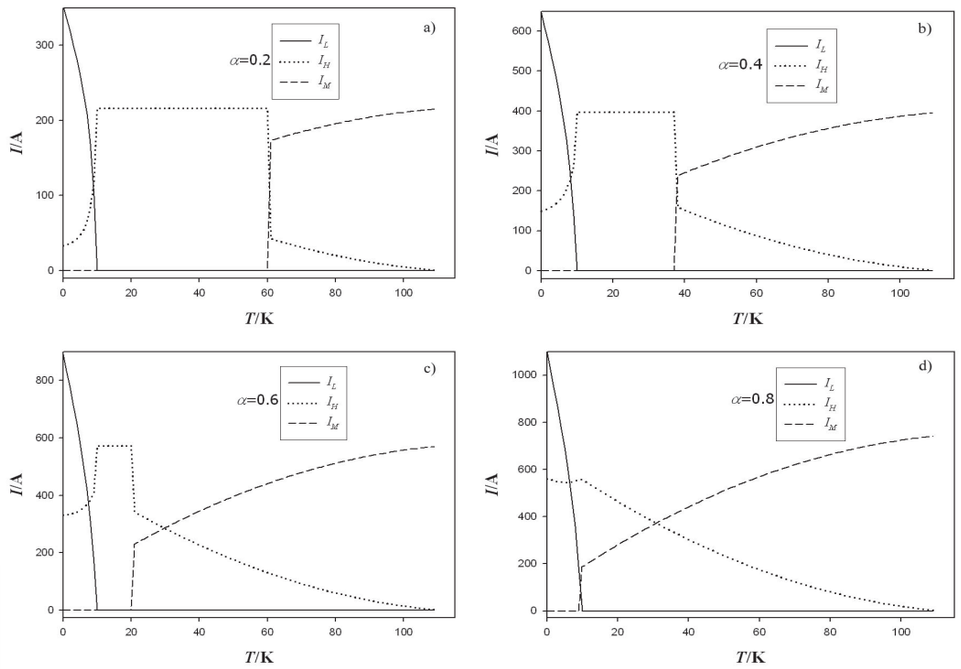


Fig. 6. The current distributions among NbTi, YBCO CC and the matrices in the hybrid superconductor vs temperature when the normalized transport current α=0.2, 0.4, 0.6, 0.8, respectively

In this simulation, $n_H$ =12 and $n_L$ =30 are adopted and assume that both of them are independence of temperature. Under conditions of normalized transport current α=0.2, 0.4, 0.6, 0.8, the temperature dependence of current distribution among three components are showed in Fig.6. With α=0.2, shown as in Fig. 6(a), the simulation results indicate that the current mainly flows in NbTi below 10 K, then transfers from NbTi to YBCO CC near above 10 K, and is totally transported by YBCO in range of 10 K through 60 K after NbTi quenching, then starts to transfer to the metal matrix gradually with temperature increasing. Finally, total current flows into the matrices after YBCO quenching completely. Figs.6(b), (c)

and (d) show the larger normalized transport current, the lower temperature of current beginning to transfer from YBCO CC to the matrices. If $I_T<I_{cH}$, the current variation in the matrices is very flat, but there is a sudden increase which can be observed when $I_T>I_{cH}$, especially at $\alpha>0.5$.

When the hybrid conductor operates below 10 K, the current ratio of NbTi to YBCO CC decreases with increasing of the normalized current and temperature, as indicated in Fig.7.

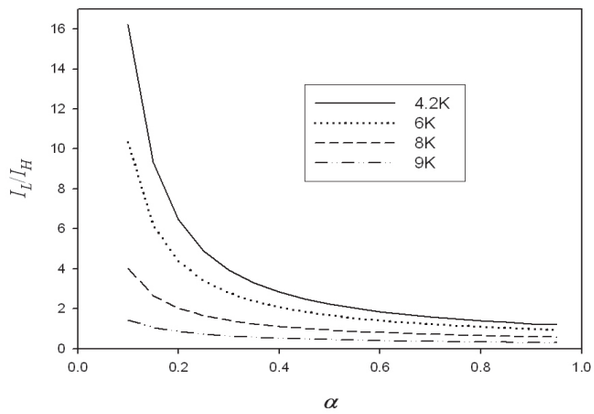


Fig. 7. The current ratio of NbTi to YBCO CC at different normalized transport currents

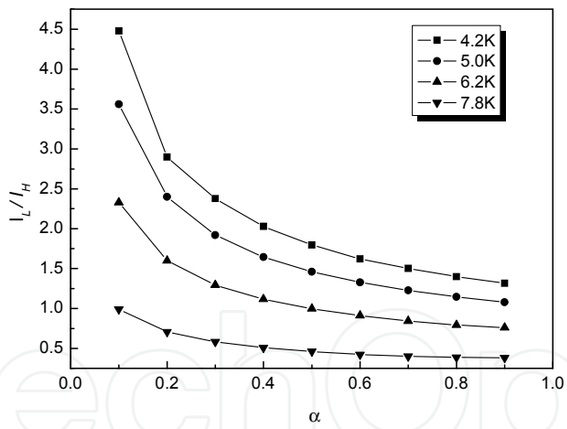


Fig. 8. Current distribution between NbTi/Cu conductor and Bi2223/Ag tapes

### 3.1.2 Current distribution of hybrid conductor made of NbTi/Cu and Bi2223/Ag

Same processing as the former hybrid conductor, this type of hybrid conductor is obtained by soldering NbTi/Cu with Bi2223/Ag. But there are much more components in matrices than the former one. Dependence of critical currents of two Bi2223/Ag tapes on temperature are approximately given by

$$I_c(T) = I_c(0)\left(1-\frac{T}{T_c}\right)^{1.4} \tag{22}$$

where $I_c(0)$=620 A, $T_c$=110 K. The critical current is $I_c$=586 A with 6 T and 4.2 K. Unlike the former hybrid conductor, the matrices in this conductor include silver, stainless steel except for Copper and solder. The relations of resistivity (Ω·m) of silver and stainless steel with temperature can be expressed as polynomial terms

$$\rho_{Ag}(T)=\begin{cases}8.5\times10^{-12}e^{0.1037T} & (4K<T\le 40K)\\ -3.4\times10^{-16}T^3+8.5\times10^{-14}T^2+7.14\times10^{-11}T-2.428\times10^{-9} & (60K<T\le 300K)\end{cases} \quad (23)$$

and

$$\rho_{ss}(T)=1.05\times10^{-12}T^2+4.72\times10^{-10}T+4.8705\times10^{-7} \quad (24)$$

The current distributions are numerically calculated in a parallel magnetic field of 6 T by using Eqs.(2)-(7), (17), (19), (20)-(24)" with Q=0 (no disturbance) when the transport current $I_T$ is smaller than its critical current in various temperatures below 8K. The results are shown in Fig.8, in which current distributions among NbTi, Bi2223 and matrices with different temperatures are indicated.

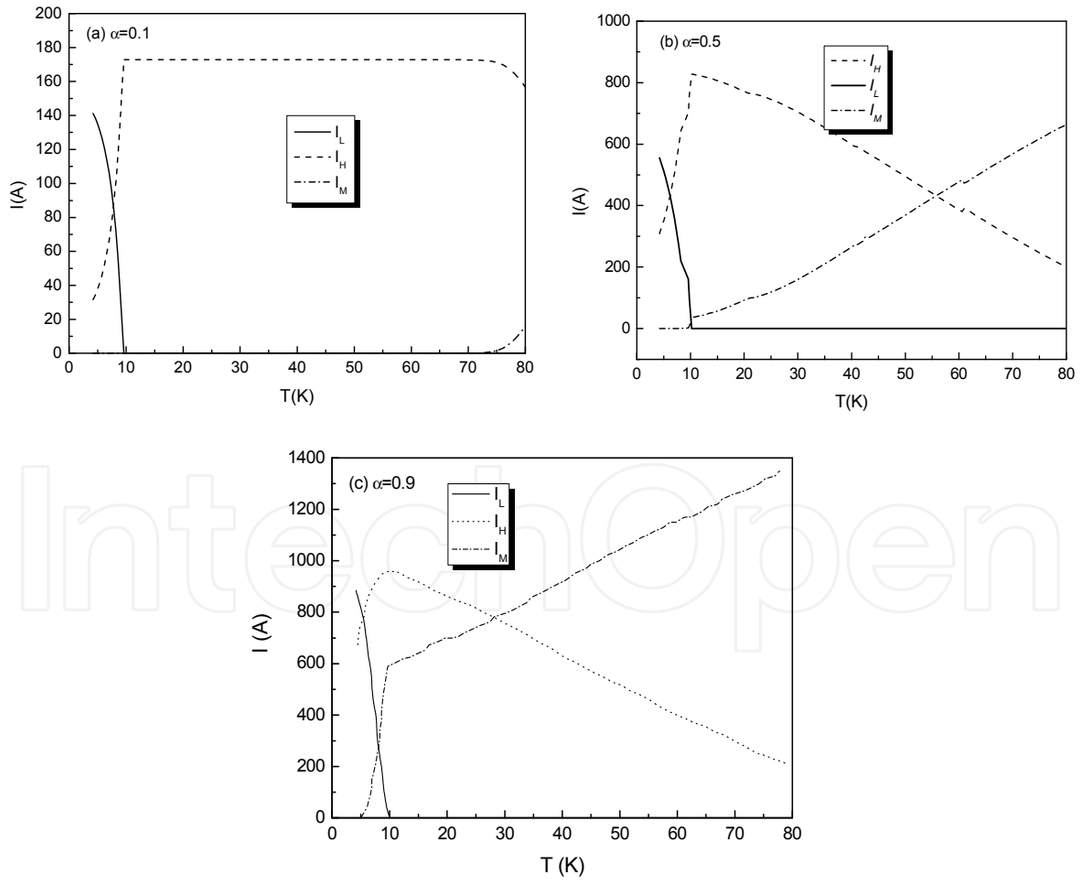


Fig. 9. Current distributions among NbTi, Bi2223 and matrices with different temperatures at α=0.1, 0.5 and 0.9

It is shown that $I_L$ decreases while $I_H$ increases with rise of temperature, which is due to the different n values in NbTi and Bi2223/Ag. Although the difference of both critical currents is not large enough at 4.2 K and 6 T, $I_L$ is larger than $I_H$ when α is smaller than 0.7. The value of $I_H$ becomes close to $I_L$ when α is close to 0.9 at about 5K, respectively. However, $I_L$ approaches to $I_H$ at 6.2K with α=0.6, and $I_L \leq I_H$ holds at 7.8 K for all values of α in the range of 0.1 through 0.9.

In order to consider the effect of the matrices on the current distribution with increasing temperature and transport current $I_T$, the current distributions among the NbTi conductor, Bi2223 tape and matrix were also simulated. Current distributions with different α 's are presented in Figs.9(a)-(c) in range of 4.2 K through 80 K.

Fig. 9(a) indicates that $I_L$ decreases but $I_H$ increases with rise of temperature when α= 0.1. $I_H$ reaches a maximum then remains constant in the range of 9.5 K through 70 K while $I_M$ is still zero for T≤70 K. If T>70 K, it gradually increases while $I_H$ decreases. $I_L$ and $I_H$ intersect each other at 7.8 K, and $I_L$ decreases to zero with temperature increasing to its critical temperature. However, $I_M$ appears in temperature T=9.5K when transport current increases to α=0.5, and then it gradually increases with temperature, as shown in Fig. 9(b). At α=0.9, the current distribution is shown in Fig. 9(c). Similar to the case of α=0.5, $I_H$ reaches its maximum at about 9.5 K then decreases gradually. But there is a difference in $I_M$'s of Figs.9(b) and (c). In Fig.9(b), $I_M$ gradually increases with temperature. However, it has a "knee point" at about 9.5K and its slope dramatically increases between 5.5 K and 9.5K, and then increases at a slower rate due to the large transport current and large n value of NbTi. Comparing with $I_L$, the rate of increase or decrease of $I_H$ is lower since Bi2223 has a lower n value.

### 3.2 Stability of the hybrid conductor

#### 3.2.1 Stability of hybrid made of NbTi/Cu and YBCO CC

In order to solve Eq. (15), the heat capacity γC (J·m$^{-3}$·K$^{-1}$) and thermal conductivity k(W·m$^{-1}$·K$^{-1}$) in all of the components including NbTi, YBCO and every kind of matrices must be known. All of them are listed as followings (Fujiwara et al, 1994)

i. NbTi

$$C_{NbTi}(T) = 0.152 + 2.10 \times 10^{-3} T^3 \tag{25}$$

With unit of J·kg$^{-1}$·K$^{-1}$, multiplied by mass density $\gamma_{NbTi}$=6550 (kg·m$^{-3}$) , (25) can be converted to volumetric heat capacity with unit (J·m$^{-3}$·K$^{-1}$).

$$k_{NbTi}(T) = \begin{cases} 0.38887 \times T^{0.1532} - 0.371 & (4K < T \leq 6K) \\ 0.13957 \times T^{0.782} - 0.4262 & (6K < T \leq 100K) \end{cases} \tag{26}$$

ii. YBCO CC

$$C_{YBCO}(T) = \begin{cases} 1.1 - 0.4T + 5 \times 10^{-2} T^2 - 4 \times 10^{-5} T^3 & (2K \leq T < 50K) \\ -125.2 + 5.6T - 1.9 \times 10^{-2} T^2 & (50 \leq T < 100K) \\ 80 + 2T - 3 \times 10^{-3} T^2 & (100K \leq T \leq 300) \end{cases} \tag{27}$$

With mass density $\gamma_{YBCO}$=6380(kg·m$^{-3}$)

$$k_{YBCO}(T)=\begin{cases}-3.5332+9.6273T-0.1282T^2+5\times10^{-4}T^3 & (2K<T\le 50K)\\ 208.45+0.2165T-5\times10^{-6}T^2 & (50<T<300K)\end{cases} \tag{28}$$

iii. Copper

$$C_{cu}(T)=7.582\times10^{-4}T^3 \qquad (4K<T\le 100K) \tag{29}$$

With mass density $\gamma_{Cu}$=8940 (kg·m$^{-3}$).

The expression for copper thermal conductivity is $k_{Cu}(T)=10^{f(T)}$ , taking Y=Log(T), the f(T) is expressed by

$$f(T)=\begin{cases}1.9153+1.7202Y-0.4146Y^2 & (4K<T\le 15K)\\ 0.8611+3.7464Y-1.3762Y^2 & (15K<T\le 23.7K)\\ -13.9115+33.952Y-21.482Y^2+4.3295Y^3 & (23.7K<T\le 100K)\end{cases} \tag{30}$$

iv. Solder (Iwasa, 1994; Jack, W. Ekin, 2007)

$$C_{solder}(T)=\begin{cases}-3.27\times10^{-2}T^2+5.3731T-20.666 & (4.2K\le T<77K)\\ -1.0\times10^{-4}T^2+1.2582T+162.01 & (77K\le T<100K)\end{cases} \tag{31}$$

With mass density $\gamma_{solder}$=7310(kg·m$^{-3)}$.

$$k(T)=\begin{cases}2\times10^{-3}T^3-0.2056T^2+6.4032T-4.008 & (4K\le T<45K)\\ 50.6 & (45K\le T<300K)\end{cases} \tag{31}$$

Substituting Eqs. (24)-(31) into Eq.(14) and considering the boundary condition (15) in adiabatic condition, the longitudinal quench propagation velocity (QPV) and the minimum quench energy (MQE) are numerically calculated by finite element method (FEM).

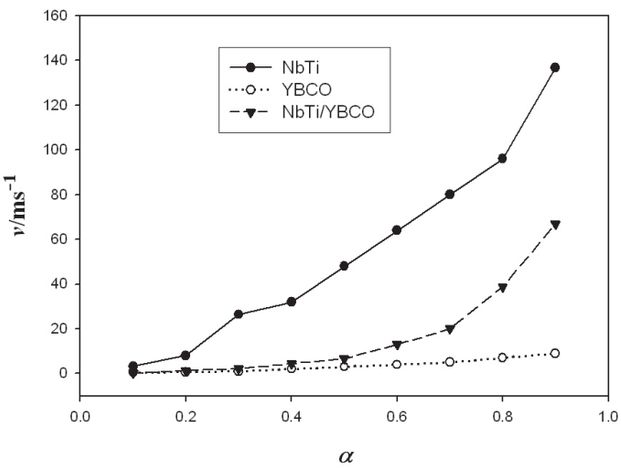


Fig. 10. The comparison of quench propagation velocities in NbTi, YBCO and NbTi/YBCO hybrid conductor with different transport currents.

The quench velocities of NbTi, YBCO and hybrid NbTi/YBCO conductor with different transport current ratios α are shown in Fig. 10, where the longitudinal QPV of NbTi is the maximum, the one in YBCO is minimum, and the QPV in hybrid NbTi/YBCO conductor is in the range of NbTi through YBCO. Therefore, the QPV of the hybrid conductor is neither faster than that of NbTi nor slower than that of YBCO CC, which is very useful for quench detection and protection of superconducting magnets.

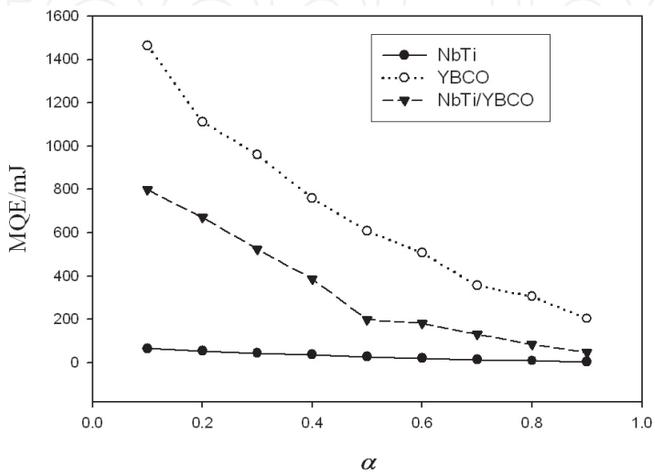


Fig. 11. The comparison of the MQE of NbTi, YBCO CC and NbTi/YBCO CC hybrid conductor with different transport currents.

Fig. 11. shows that the MQE of NbTi/YBCO CC hybrid conductor is in range of NbTi through YBCO CC with order of magnitude of mJ (several kJ·m$^{-3}$). When α<0.5, the MQE of the hybrid conductor is parallel to that of YBCO CC. An inflection point is observed in the curve at α=0.5, which is perhaps related to the transport current which exceeds the critical current of NbTi. When α>0.5, the MQE is close to that of NbTi. Generally, the MQE of NbTi/YBCO CC hybrid conductor is much larger than that of pure NbTi, which indicates that the stability of superconductor can be improved compared with pure NbTi/Cu wire.

### 3.2.2 Stability of hybrid made of NbTi/Cu and Bi2223/Ag tape

In section 3.1.1, the heat capacity and thermal conductivity of NbTi, YBCO, copper and solder are given, we list the heat capacity C (J·kg$^{-1}$·K$^{-1}$·) and thermal conductivity k(W·m$^{-1}$·K$^{-1}$) of other materials including Bi2223, stainless steel, silver.

i. Bi2223

$$C_{Bi2223}(T)=\begin{cases}4.5683\times10^{-3}T^{3} & (T\le 10K)\\ -3.088+0.64996T+8.23239\times10^{-3}T^{2}+3.2406\times10^{-4}T^{3} & (10K\le T\le 40K)\\ -58.32+3.18672T-7.8786\times10^{-3}T^{2}+6.5556\times10^{-6}T^{3} & (40K\le T\le 300K)\end{cases} \quad (33)$$

With mass density $\gamma_{Bi2223}$=6500(kg·m$^{-3}$).

$$k_{Bi2223}(T)=\begin{cases}0.02T & (T\le 55K)\\ \left(\begin{array}{l}0.474+8.43\times10^{-3}T+3.25\times10^{-4}T^2-6.595\times10^{-6}T^3\\ +2.81\times10^{-8}T^4\end{array}\right) & (55K<T\le 77K)\\ \left(\begin{array}{l}0.195+9.424\times10^{-3}T+3.4\times10^{-4}T^2-6.237\times10^{-6}T^3\\ +2.673\times10^{-8}T^4\end{array}\right) & (77K<T<113K)\\ \left(\begin{array}{l}4.749-0.102T+9.901\times10^{-4}T^2-4.167\times10^{-6}T^3\\ +6.531\times10^{-9}T^4\end{array}\right) & (113K\le T<200K)\end{cases} \quad (34)$$

ii. Silver

$$C_{Ag}(T)=\begin{cases}8.41\times10^{-4}T^3+5.10\times10^{-2}T^2-0.5566T+1.6341 & (4K<T\le 18K)\\ 2.341\times10^{-5}T^3-1.674\times10^{-2}T^2+3.8384T-50.775 & (18K<T\le 300K)\end{cases} \quad (35)$$

With mass density $\gamma_{Ag}$=10490 (kg·m$^{-3}$).

$$k_{Ag}(T)=\begin{cases}43.343\times T^3-1227.2T^2+10513T-10254 & (4K<T\le 10K)\\ -0.6174T^3+72.264T^2-2816.5T+37594 & (10K<T\le 38K)\\ -0.0179T^3+3.6865T^2-253.64T+6292.2 & (38K<T\le 50K)\\ -1.3\times10^{-2}T^2-0.825T+640.3 & (50K<T\le 100K)\\ 420 & (100K<T\le 300K)\end{cases} \quad (36)$$

iii. Stainless steel (304L)

$$C_{ss}(T)=\begin{cases}2\times10^{-6}T^3+1.59\times10^{-2}T^2+0.2644T+0.4089 & (4K<T\le 30K)\\ 3.114\times10^{-4}T^2+0.7171T-1.7843 & (30K<T\le 300K)\end{cases} \quad (37)$$

With mass density $\gamma_{ss}$=7900(kg·m$^{-3}$).

$$k_{ss}(T)=2.7041\times10^{-9}T^3-3.3219\times10^{-4}T^2+0.126T-0.1877 \quad (4K\le T\le 300K) \quad (38)$$

In this section, the longitudinal QPV and MQE are numerically simulated by solving Eq.(8) in combination with Eqs. (10)-(12), (16), (25), (26) and (29)-(38) under adiabatic conditions. Figs.12(a)-(c) show the temperature profiles at locations of 20 mm, 40 mm, 60 mm and 80 mm from the center with different external disturbances and transport currents. The variations of n values with temperature are not considered in simulation. The hybrid conductor was tested in magnetic field of 6 T which was applied for reducing its critical current in measurement. The dependence of n values on temperature is very difficult to obtain by experiment with supplying so high a transport current and background magnet. Therefore, we used the constant n values in simulation. Usually, the n values will decrease with increasing temperature, but we took n values approximately constant with fixed magnetic field regardless of influence of temperature in order to simplify calculation. In future, we should take NbTi and Bi2223 with small $I_c$ in experiment within magnet bore in which temperature can be changed. Or the n values are measured by contact-free methods, like those methods adopted in HTS at 77 K (Wang et al, 2004; Fukumoto et al, 2004).

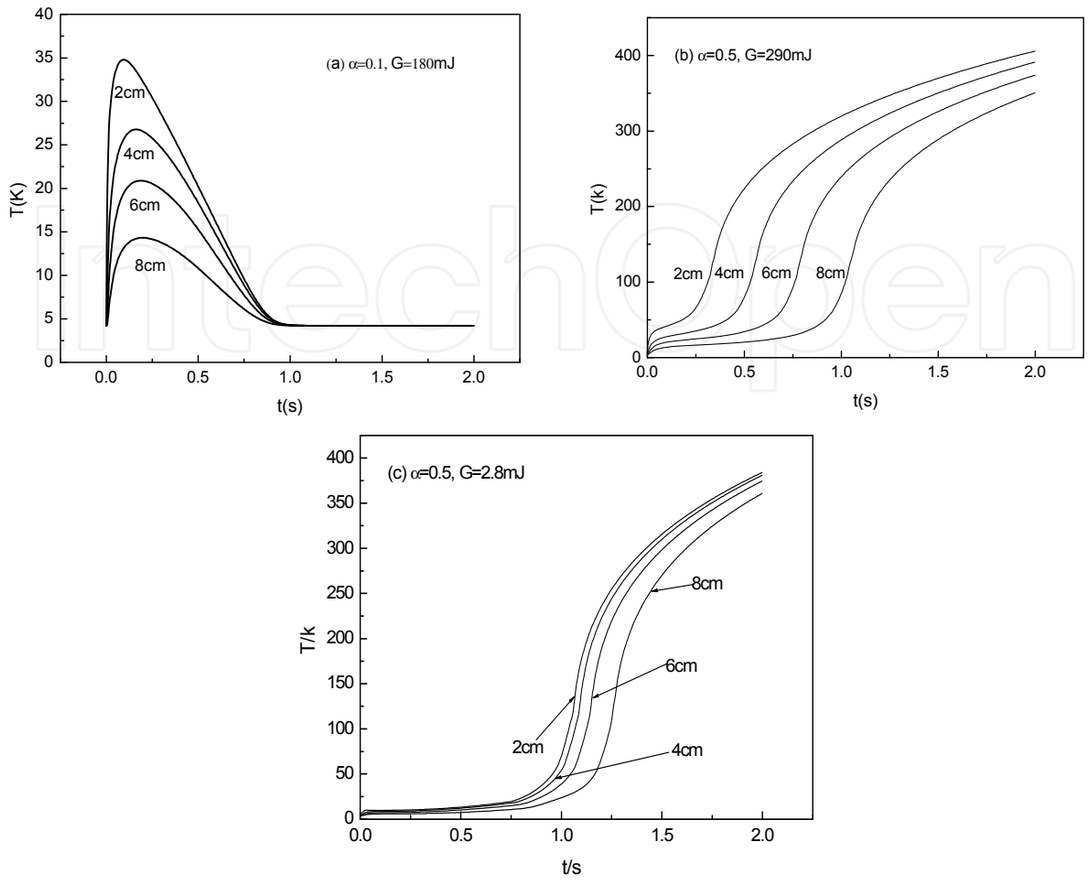


Fig. 12. Temperature profiles of the hybrid conductor with different transport current

When $I_T$ is small (α=0.1) and there is a disturbance G=180mJ (~192kJ·m$^{-3}$), though the maximum temperature reaches to 35K, the quench doesn't propagate. Once the disturbance disappears, the hybrid conductor recovers to its original state at 4.2 K, as shown in Fig. 12(a). The reason is that the extra current in the NbTi transfers to the Bi2223 even though the temperature is far above the critical temperature of NbTi, but is still far below the critical current of Bi2223. There is no Joule heat generation in the hybrid conductor even though $I_T$ is applied. For disturbances of G=290mJ (~310kJ/m$^3$) and 2.8mJ (~3kJ·m$^{-3}$) with transport currents α=0.3 and 0.5, the quench does propagate and the results are shown in Figs. 12(b) and (c) to indicate that the quench process can not recover.

Figs. 13 and 14 present the longitudinal QPV ($V_Q$) and MQE ($Q_E$)of three types of composite conductors (NbTi, hybrid NbTi/Bi2223 and Bi2223) with different normalized transport current factor α. The longitudinal QPV increases with increasing α. Among the three types of conductors, $V_q$ in NbTi/Cu is the largest (~10$^2$ m/s), the one in Bi2223 is the lowest (~10$^{-2}$-10$^{-1}$ m/s), but $V_q$ in the hybrid NbTi/Bi2223 falls in the range of about 10$^{-1}$ m/s through10 m/s for α≥0.4. On the other hand, $Q_E$ decreases with increasing α. $Q_E$ of Bi2223 is the largest (~10$^3$mJ), the lowest in NbTi (~10$^{-2}$-1 mJ) and falls on the range of 1 mJ through 10$^3$ mJ in the hybrid conductor. In the case of α≤0.4, $Q_E$ in the NbTi/Bi2223 is more than 100mJ but significantly decreases while α is in the range of 0.4 through 0.5, and then it decreases gradually with increasing α. Nevertheless, $Q_E$ of the hybrid conductor is at least more than

one order of magnitude higher than the NbTi. Therefore, the stability of the hybrid conductor is improved greatly comparing with the NbTi conductor.
More exact simulation should be based on three-dimensional model in which the temperature distribution in cross-section can be numerically analyzed. This method will be used in future research.

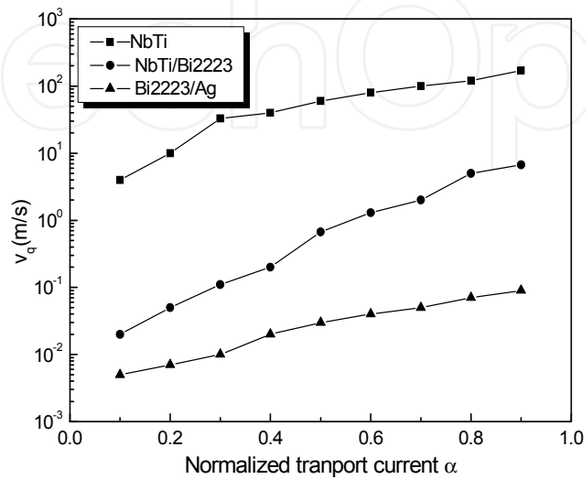


Fig. 13. Longitudinal QPV (Vq) of three types of conductors

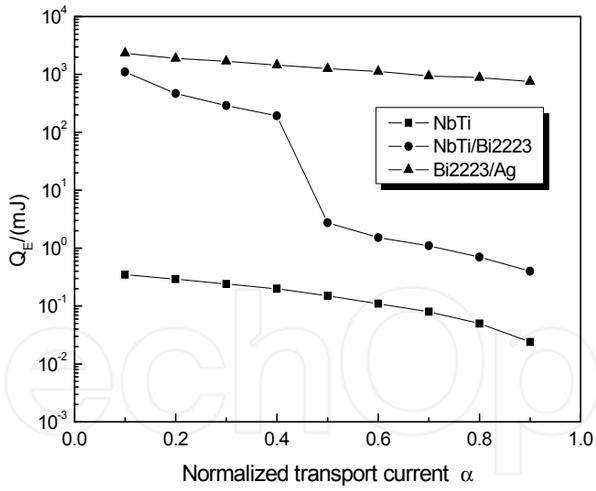


Fig. 14. MQE $Q_E$ of three types of conductors

## 4. Experiment

The hybrid conductor was prepared by soldering two Bi2223/Ag tapes onto one NbTi/Cu conductor by use of Indium-Silver alloy solder under 200 $^0$C in order to avoid degradation of Bi2223/Ag tape (Wang, 2009). One heater and two Rh-Fe thermometers were attached to the hybrid conductor. Next, the hybrid sample was wound by 10 layers of fiber glass tape and then immersed into epoxy resin in order to simulate the quasi-adiabatic environment.

The total length of the hybrid was 900 mm and was wound on a FRP bobbin with diameter of 70 mm. The main parameters of each conductor were also listed previously in Table 1 and the sample is shown as Fig.15.

A schematic diagram of the experimental set-up is illustrated in Fig.16. The hybrid sample was tested under a background field of 6 T provided by an NbTi NMR magnet with a core of diameter 88.6 mm and homogeneity of $1.7\times10^{-7}$ in a 10 mm×10 mm spherical space, which ensured that the sample was located in the same field. The total length of the homogeneity region in axial orientation was 200 mm. The magnet was composed of 3 main coils and 2 compensated coils wound using NbTi/Cu composite wire. The heater, bifilar wound non-inductively by copper-manganese wire with a diameter of 0.1 mm, had a resistance of 69.7 Ω at 4.2 K.

Fig. 15. Prepared sample

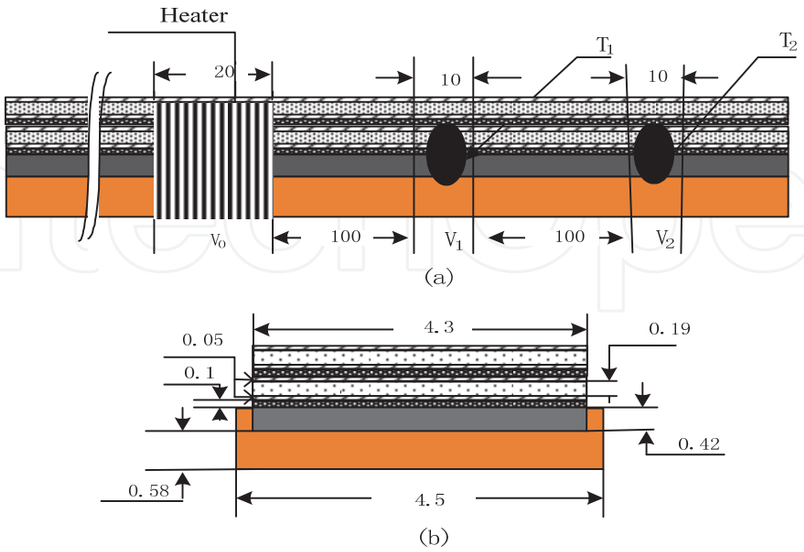


Fig. 16. Schematic of sample test arrangement. (a) and (b) are front-view and side-view of the hybrid conductor, respectively. $T_1$ and $T_2$ refer to temperature sensors. unit: mm.

The tests were performed in a 4.2 K helium bath and the magnet was excited with 6 T in all experiments. The quench voltage and temperature profiles were measured by triggering the heater with rectangular waveforms of different durations and amplitudes. Since 800 A was the limit of our power supply, the maximum transport current in sample was 800 A in this section.

## 5. Results and discussions

When a transport current of 400A was supplied in a background magnetic field of 6T, the quench voltage and temperature profiles are shown in Figs. 17 and 18, respectively,. The duration of power from the heater was 0.4s and the amplitude was 0.3A; therefore, the disturbance energy from the heater was 2.5J. When the heater was triggered, only the central part of the sample quenched, $V_1$ appeared slightly, but $V_2$ remained the same. The

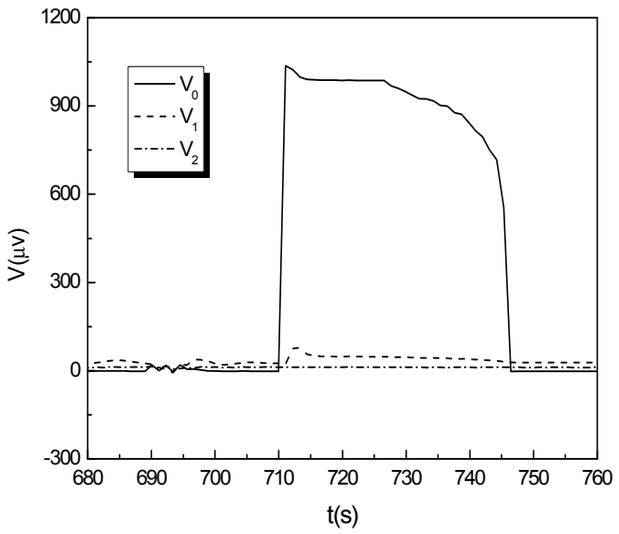


Fig. 17. Voltage profiles with impulse duration of 0.4 s and amplitude of 0.3 A

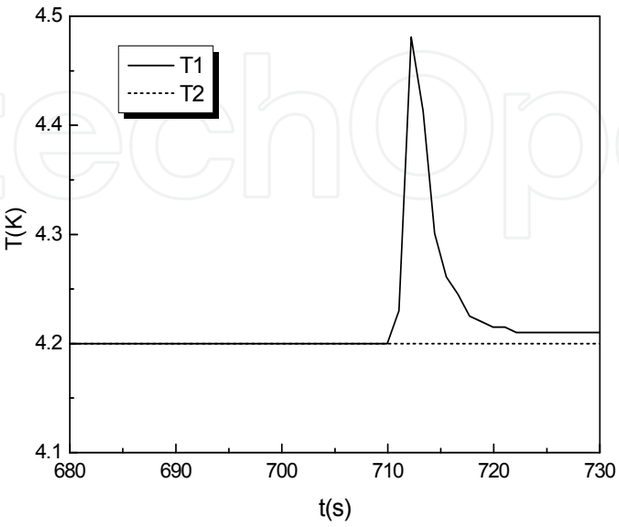


Fig. 18. Temperature profile with impulse duration of 0.4 s and amplitude of 0.3 A

temperature profiles with a peak of 4.4 K were different from voltages and the temperature of $T_2$ kept constant, which indicates that the quench recovered and there was no quench propagation during the triggering.

In order to measure the quench propagation, the transport current 800 A was applied, the triggering duration and amplitude were 59 ms and 0.1 A, respectively, i.e. the triggering energy is 41.12 mJ. The voltage and temperature profiles are presented in Figs. 19 and 20. When heater was triggered, three parts of the sample quenched, $V_1$ is slightly larger than $V_2$, the temperature profiles with maximum 11 K are similar to the voltages, which mean that the quench propagates. The order of the $V_q$ is 10 m/s which is higher than the Bi2223/Ag tape (Dresner, 1993). $Q_E$ has order of several tens of mJ, which are much larger than those of the NbTi/Cu conductor (Frederic et al, 2006). On contrary to 400 A, quench propagation does take place; $Q_E$ and $V_q$ are 41.12 mJ and 10 cm/s, respectively, which qualitatively agree with the simulated results in section 3.2.2 in case of normalized transport current $\alpha$=0.5, though the experimental results are smaller than simulations. The differences between the experiment and simulation result from the assumptions of adiabatic conditions and constant n values in different temperatures. Practically, the quasi-adiabatic condition in the experiment is just an approximate and dependence of the n values on temperature and magnetic field should be included. In future, an experiment including normal zone propagation (NZP), $V_q$ and $Q_E$ should be performed by using cryo-cooler and LTS with lower critical current in order to obtain the quench parameters exactly. Furthermore, a three-dimensional model should be adopted. The stability of other types of hybrid conductor, such as LTS (NbTi, $Nb_3Sn$) /$MgB_2$, HTS(BSCCO, YBCO)/$MgB_2$ and $Nb_3Sn$/HTS, could be also needed to study by simulation and experiment.

Additionally, the variations of n values with temperature and magnetic field should be taken account into consideration and measured possibly by contact-free methods similar with those used in HTS tapes (Wang et al, 2004; Fukumoto et al, 2004). This work will need to conduct in near future.

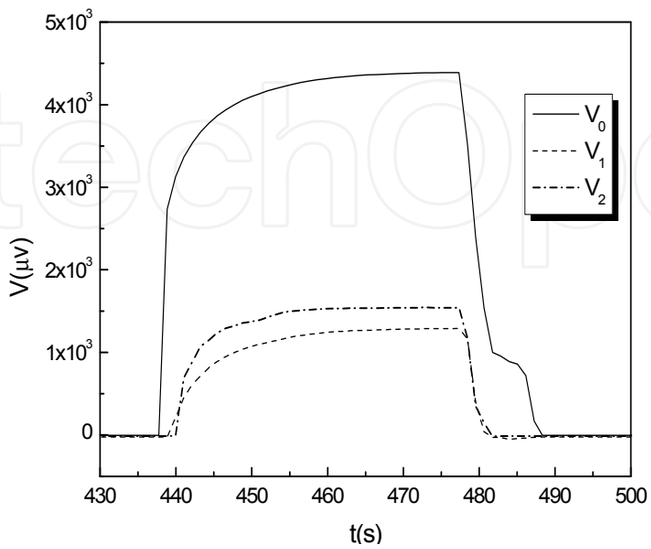


Fig. 19. Voltage profiles with impulse duration of 59 ms and amplitude of 0.1 A.

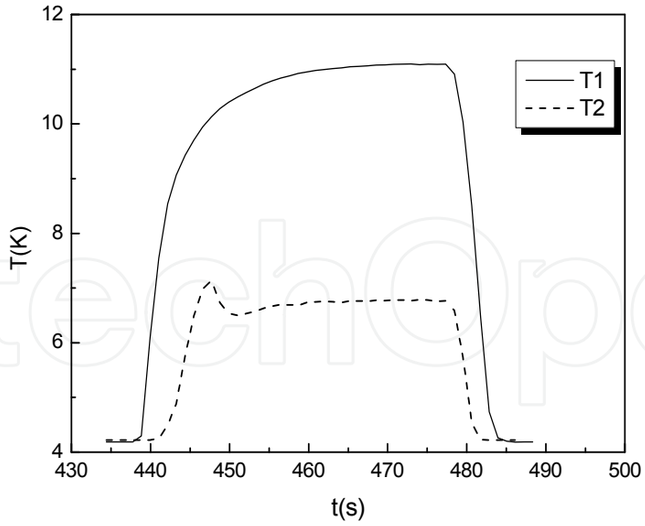


Fig. 20. Temperature profiles with impulse duration of 59 ms and amplitude of 0.1A

## 6. Conclusions

The current distribution and stability of LTS/HTS hybrid conductor, which is made of NbTi wire and YBCO coated-conductor, are numerically calculated. The results indicate that the current in LTS is larger than in HTS if both of them have the approximate critical currents and the current ratio of NbTi to YBCO CC decreases with increase of transport current and temperature when the hybrid conductor operates. On the other hand, the longitudinal quench propagation velocity is in the range of NbTi through HTS, which is very important for quench detection and protection of superconducting magnets. Finally, the MQE ($Q_E$) in the hybrid conductor is much higher than in NbTi wire and smaller than in YBCO CC conductor, which shows that the thermal stability of superconductor can be improved.

Based on the concept of a hybrid NbTi/Bi2223 conductor and power-law models, the current distribution was simulated numerically. Since NbTi has a higher n value than Bi2223, most of current initially flows through NbTi while the ratio of current in Bi2223 to that in NbTi increases with rise of temperature and transport current below their total critical current. The stability of the hybrid conductor was simulated using one-dimensional model. The results show that the $V_q$ of the hybrid conductor is smaller, but the $Q_E$ is bigger than NbTi conductor, which indicates that the stability of the hybrid superconducting conductor is improved. Simultaneously, a high engineering current density was also achieved. A short sample, made of Bi2223/Ag stainless-steel enforced multifilamentary tape and NbTi/Cu, was prepared and tested successfully at 4.2 K. The results are in qualitative agreement with the simulated ones.

With improving on their stability and engineering critical current compared with conventional LTS and HTS, the hybrid conductors have potential application in mid- and large scale magnet and particularly in the cryo-cooled conduction magnet application.

In future, the cryocooler-cooled conduction should be adopted in the experiments, and a three-dimensional model with n values depending on temperature and magnetic field and

its orientation should be taken into account to improve the present numerical results. Stability in other types of hybrid conductor, such as (NbTi, $NbSn_3$)/$MgB_2$ and (NbTi, $NbSn_3$)/YBCO CC, should be also valuable for study in next step.

## 7. Acknowledgements

The author thanks Ms. Weiwei Zhou, Dr. Wei Pi, Prof. Xiaojin Guan and Dr. Hongwei Liu for their contributions to the research included in the chapter. This work was supported in part by the National Natural Science Foundation of China under grant No.51077051 and Specialized Research Fund for the Doctoral Program of Higher Education under grant No.D00033.

## 8. References

Dresner, L. (1993) Stability and protection of Ag/BSCCO magnets operated in the 20-40 K range. *Cryogenics*, Vol.33, pp 900-909

Dutoit, B; Sjoestroem, M. & Stavrev, S. (1999) Bi(2223) Ag sheathed tape Ic and exponent n characterization and modeling under DC applied magnetic field. *IEEE Trans. Appl. Supercond*., Vol.9, No.2, pp. 809-812

Frederic, T, Frederic, A & Amaud, D. (2006) Investigation of the stability of Cu/NbTi multifilament composite wires. *IEEE Trans. Appl. Supercond*. Vol.16, No.2, pp. 1712-1716

Fukumoto, Y; Kiuchi, M. & Otabe, E. S. (2004) Evolution of E-J characteristics of YBCO coated–conductor by AC inductive method using third-harmonic voltage. *Physica C*, Vol. 412-414, pp 1036-1040

Fujiwara, T; Ohnishi, T; Noto, K; Sugita, K. & Yamamoto, J. (1994) Analysis on influence of temporal and spatial profiles of disturbance on stability of pooled-cooled superconductors. *IEEE Trans Appl. Supercond*., Vol.4, No. 2, pp. 56-60.

Gourab, B.; Nagato, Y. & Tsutomu, H. (2006) Stability measurements of LTS/HTS hybrid superconductors. Fusion Eng. Des., Vol. 81, pp. 2485-2489

Iwasa, Y. (1994) *Case studies in superconducting magnet*. Plenum Press, New York and London.

Jack, W. Ekin. (2007) *Experimental Techniques for Low-Temperature Measurement*. Oxford University Press Inc., New York.

Rimikis, A.; Kimmich, R. & Schneider, Th. (2000) Investigation of n-values of composite superconductors. *IEEE Trans Appl. Supercond*., Vol.10, No.1, pp.1239-1242

Torii, S.; Akita, S.; Iijima, Y.; Takeda, K. & Saitoh, T. (2001) Transport current properties of Y-Ba-cu-O tape above critical current region. *IEEE Trans Appl. Supercond*., Vol.11, No.1, pp. 1844-1847

Wang, Y. S. ; Zhao, X and Han, J. J. (2004) A type of LTS/HTS composite superconducting wire or tape. Chinese patent (ZL200410048208.8 (In Chinese).

Wang, Y. S.; Zhang, F. Y. & Gao, Z. Y. (2009) Development of a high-temperature superconducting bus conductor with large current capacity. *Supercond. Sci. Technol*., Vol.22, 055018 (5pp)

Wang, Y. S.; Lu, Y. & Xiao, L.Y. (2003) Index number (n) measurements on BSCCO tapes using a contact-free method. *Supercond. Sci. Technol*. Vol.16, pp. 628-63

Wilson, M. N. (1983). *Supercnducting Magnet*. Clarendon Press Oxford, London.

Yasahiko, I.& Hidefumi, K. (1995) Critical current density and n-value of NbTi wires at low field. *IEEE Trans Appl. Supercond*., Vol.5, No.2, pp. 1201-1204

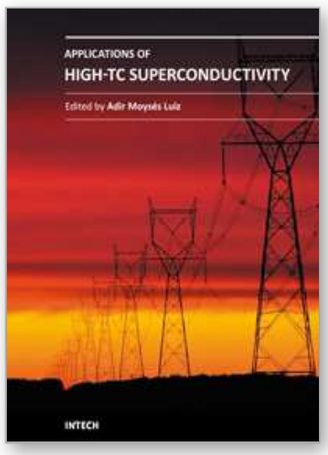


**Applications of High-Tc Superconductivity**
Edited by Dr. Adir Luiz

ISBN 978-953-307-308-8
Hard cover, 260 pages
**Publisher** InTech
**Published online** 27, June, 2011
**Published in print edition** June, 2011

This book is a collection of the chapters intended to study only practical applications of HTS materials. You will find here a great number of research on actual applications of HTS as well as possible future applications of HTS. Depending on the strength of the applied magnetic field, applications of HTS may be divided in two groups: large scale applications (large magnetic fields) and small scale applications (small magnetic fields). 12 chapters in the book are fascinating studies about large scale applications as well as small scale applications of HTS. Some chapters are presenting interesting research on the synthesis of special materials that may be useful in practical applications of HTS. There are also research about properties of high-Tc superconductors and experimental research about HTS materials with potential applications. The future of practical applications of HTS materials is very exciting. I hope that this book will be useful in the research of new radical solutions for practical applications of HTS materials and that it will encourage further experimental research of HTS materials with potential technological applications.



INTECH
open science | open minds

**InTech Europe**
University Campus STeP Ri
Slavka Krautzeka 83/A
51000 Rijeka, Croatia
Phone: +385 (51) 770 447
Fax: +385 (51) 686 166
www.intechopen.com

**InTech China**
Unit 405, Office Block, Hotel Equatorial Shanghai
No.65, Yan An Road (West), Shanghai, 200040, China
中国上海市延安西路65号上海国际贵都大饭店办公楼405单元
Phone: +86-21-62489820
Fax: +86-21-62489821

IntechOpen